Targeting Ballistic Lunar Capture Trajectories Using Periodic Orbits in the Sun-Earth CRTBP

Paul Ricord Griesemer[1] and Cesar Ocampo[2]
The University of Texas at Austin, Austin, Texas, 78712

and
D. S. Cooley[3]
NASA Goddard Space Flight Center, Greenbelt, Maryland, 20771

A particular periodic orbit in the Earth-Sun circular restricted three body problem is shown to have the characteristics needed for a ballistic lunar capture transfer. An injection from a circular parking orbit into the periodic orbit serves as an initial guess for a targeting algorithm. By targeting appropriate parameters incrementally in increasingly complicated force models and using precise derivatives calculated from the state transition matrix, a reliable algorithm is produced. Ballistic lunar capture trajectories in restricted four body systems are shown to be able to be produced in a systematic way.

Nomenclature

WSB	=	weak stability boundary
LEO	=	low Earth orbit
CRTBP	=	circular restricted three body problem
RTBP	=	restricted three body problem
RFBP	=	restricted four body problem
μ_s	=	gravitational parameter of the Sun
μ_e	=	gravitational parameter of the Earth
μ_m	=	gravitational parameter of the Moon
μ	=	mass ratio in the circular restricted three body problem
c	=	Jacobi constant in the circular restricted three body problem
α	=	orientation angle of a circular parking orbit
β	=	orientation angle of a circular parking orbit
γ	=	orientation angle of a circular parking orbit
ΔV	=	magnitude of the transfer trajectory insertion burn
$\mathbf{r}$	=	position vector of a spacecraft in a coordinate system centered on the Earth-Moon barycenter
$\mathbf{v}$	=	velocity vector of a spacecraft in a coordinate system centered on the Earth-Moon barycenter
$\mathbf{a}$	=	acceleration vector of a spacecraft in a coordinate system centered on the Earth-Moon barycenter
$\mathbf{r}_m$	=	position vector of the Moon in a coordinate system centered on the Earth-Moon barycenter
$\mathbf{r}_s$	=	position vector of the Sun in a coordinate system centered on the Earth-Moon barycenter
$\mathbf{r}_{L2}$	=	position vector of L_2
$\mathbf{r}_{sc/s}$	=	position vector of a spacecraft relative to the Sun
$\mathbf{r}_{sc/e}$	=	position vector of a spacecraft relative to the Earth
$\mathbf{r}_{sc/m}$	=	position vector of a spacecraft relative to the Moon

[1] Graduate Student, Department of Aerospace Engineering and Engineering Mechanics, 1 University Station C0600, The University of Texas, Austin, TX 78712.
[2] Associate Professor, Department of Aerospace Engineering and Engineering Mechanics, 1 University Station C0600, The University of Texas, Austin, TX 78712.
[3] Aerospace Engineer, Flight Dynamics Analysis Branch, Guidance, Navigation and Control Center, NASA Goddard Space Flight Center, Mailstop 595.0, Greenbelt, MD 20771.

$r_{L_2/m}$	=	distance of L_2 from the Moon
$\mathbf{x}_p$	=	vector of free parameters in the targeting and optimization algorithms
$\boldsymbol{c}$	=	constraint vector in the targeting and optimization algorithms
J	=	performance index in the optimization algorithm
KE_m	=	Keplerian energy with respect to the Moon
$\mathbf{X}$	=	state vector
$\Phi(t_f,t_0)$	=	state transition matrix
$F(t)$	=	state propagation matrix
f_m	=	true anomaly in a Moon-centered coordinate frame

Introduction

A ballistic lunar capture trajectory is characterized by a spacecraft transitioning from a hyperbolic lunar orbit into an elliptical lunar orbit without the need of a maneuver at the time of transition. The trajectories were initially developed using the concept of the weak stability boundary [1, 2] (WSB), a chaotic region of phase space that exists around masses in multi-body problems. Trajectories of this type were first developed by Belbruno in 1987 [1]. Belbruno and Miller [2] were able to use the WSB in combination with the Sun's gravitational influence to successfully place a satellite in lunar orbit in 1991. Presented here is a new method of targeting impulsive ballistic lunar capture transfers from low Earth orbit using a particular family of periodic orbits in the Sun-Earth circular restricted three body problem (CRTBP).

Several methods of designing ballistic lunar capture transfers have been documented [3-11]. Belbruno and Carrico [3] have presented a two dimensional, user-in-the-loop forward targeting algorithm for transfers that approach the Moon along an orbit that has an apogee that is much greater than the distance from the Earth to the Moon. Yamakawa, et al. [4] used a shooting method to produce similar transfers in the planar restricted four body problem (RFBP). Additional algorithms exist that utilize the invariant manifolds associated with libration point orbits in the Sun-Earth and Earth-Moon circular restricted three body problems. For example, Koon, et al. [5] targeted ballistic lunar capture trajectories by finding intersections of these invariant manifolds. Similarly, Yamato and Spencer [6] approximated the invariant manifolds in a perturbed CRTBP, yielding transit orbits. Parker and Lo [7] have categorized families of ballistic lunar capture trajectories found from invariant manifolds with the intention of allowing a mission planner to choose appropriate trajectories for specific missions. Alternatively, Biesbroek et al. [8] have used genetic algorithms to successfully find WSB trajectories. Finally, Yagasaki [9] has created a non-linear boundary value problem that obtains a solution by beginning with an elliptic arc in the two body problem (mass parameters of the Sun and Moon equal to zero), and iterating the solution with increasing mass parameters of the Sun and Moon until the real-world solution is obtained.

Other low energy targeting methods exist that do not rely on solar gravitational effects. The trajectories that these transfers target approach the Moon from the direction of the interior Earth-Moon Lagrange point. Bolt and Meiss [10] developed a targeting scheme in the Earth-Moon planar circular restricted three body problem that relies on recurrence of chaotic trajectories. Macau and Grebogi [11] used a similar method to target transfers to the moon through chaotic spaces in the restricted three body problem through elimination of recurrent orbits, however, improved transfer times over Bolt and Meiss were achieved at the expense of a second maneuver and higher fuel costs. Both of these methods rely on very large parking orbits around the Earth to achieve a low energy impulsive transfer without the need of a solar perturbation. Mengali and Quarta [12] also disregard the solar gravitational influence when they compare their planar three body bi-impulsive method to WSB transfers.

The targeting of ballistic lunar capture trajectories poses problems because of the chaotic nature of the trajectory and the complexity of the four body dynamics that are required to produce them. The WSB is by definition a chaotic region in phase space where small changes in the state of a spacecraft will lead to large variations in its trajectory. In addition, ballistic lunar captures that rely on a single main impulsive maneuver to transfer from the Earth to the Moon require the gravitational dynamics of the Sun, Earth, and Moon. The four body dynamical system makes systematic convergence to ballistic lunar capture trajectories problematic.

Attempts have been made to use simpler dynamics to understand ballistic lunar capture trajectories for the purpose of creating initial guesses accurate enough to converge to solutions in a numerical targeting scheme. Ivashkin, [13] for example, has compared them to bi-elliptic transfers in a central body gravity field. Here, the solar perturbation of the Earth-centered two body problem provides the intermediate ΔV that increases the perigee distance of the orbit. From Lidov, [14] an estimation of the effect of this perturbation on the perigee distance can be made. Although the comparison of a bi-elliptic transfer with a ballistic lunar capture trajectory has been shown by these authors to be geometrically appropriate, the dynamics of the ballistic lunar capture trajectory can be better demonstrated in a three body model.

The solar effect on perigee can be seen in a family of periodic orbits in the Sun-Earth circular restricted three body problem. These periodic orbits explicitly exhibit the influence of the Sun on the low energy transfers. A targeting algorithm is described that uses a particular member of a family, documented by Markellos [15] as family $f16$, as a generating trajectory for an Earth-Moon transfer in the restricted four body problem. The algorithm overcomes the stated difficulties in numerically seeking ballistic lunar capture trajectories by using an incremental

approach from an appropriate initial guess and precise derivatives based on the state transition matrix. The given parameters for the algorithm are the initial transfer date and the properties of a low Earth parking orbit. Using the generating trajectory as an initial guess, the complexities of the four body problem are added to the targeting algorithm incrementally until the final trajectory is converged upon.

Circular Restricted Three Body Problem

The reference trajectory for the targeting algorithm is developed in the Sun-Earth circular restricted three body problem [16]. In this system, the spacecraft is assumed to be a vehicle of infinitesimally small mass. The motion of the spacecraft is governed by two bodies, the Sun and the Earth, both assumed to be point masses. The primary body in the system is the Sun, with normalized mass equal to 1-μ, and the secondary body is an object with the combined mass of the Earth and the Moon located at the Earth-Moon barycenter with normalized mass equal to μ, shown in Eq. 1.

$$\mu = \frac{\mu_e + \mu_m}{\mu_e + \mu_m + \mu_s} \tag{1}$$

The distance unit in the CRTBP is scaled to the average distance from the Sun to the Earth-Moon barycenter. A rotating coordinate system is established with the Sun and the Earth-Moon body held fixed on the x-axis, with the Earth-Moon body at the origin and the Sun located at x = -1. Assuming the Earth-Moon body orbits the Sun in a circular orbit, the coordinate frame rotates at a constant angular velocity, ω. The time unit is scaled such that ω =1. The motion of the spacecraft in the CRTBP defined above is governed by Eq. 2,

$$\ddot{\mathbf{r}} = \frac{1-\mu}{r_1^3}\begin{pmatrix} r_x+1 \\ r_y \\ r_z \end{pmatrix} - \frac{\mu}{r_2}\begin{pmatrix} r_x \\ r_y \\ r_z \end{pmatrix} + 2\begin{pmatrix} \dot{r}_y \\ -\dot{r}_x \\ 0 \end{pmatrix} + \begin{pmatrix} r_x+1-\mu \\ r_y \\ 0 \end{pmatrix}, \tag{2}$$

where the vector $\mathbf{r}$ is the position vector in the CRTBP coordinates described above.

An integral of motion known in the system, the Jacobi integral, is shown in Eq. 3. The mass parameter, μ, for the system with the Sun as the primary and the Earth and Moon combined into a single secondary body is 3.040364489 x 10^{-6}.

$$c = \left(r_x + 1 - \mu\right)^2 + {r_y}^2 + 2\frac{1-\mu}{r_1} + 2\frac{\mu}{r_2} - \left({\dot{r}_x}^2 + {\dot{r}_y}^2 + {\dot{r}_z}^2\right) \tag{3}$$

Family *f*16 Periodic Orbits

In the three body problem it is useful to look at periodic orbits as a tool for understanding the dynamics. According to the conjecture by Poincaré [17], the population of periodic orbits in the CRTBP is dense; ensuring that for every orbit there is a periodic orbit an infinitesimally small distance away in phase space. Here, periodic orbits around the secondary body (in this system the Earth-Moon combined mass) are used to demonstrate perigee increasing effects of the Sun on the spacecraft. Markellos [15] provided a survey of families of periodic orbits in the CRTBP. If Markellos's family *f* is extended such that the trajectories pass nearer to the secondary body, periodic orbits can be generated that have the desired effects on the perigee radii of the orbit. Fig. 1 shows an example of such an orbit from family *f*16 in Markellos's catalog. The trajectory is shown in a rotating reference frame centered on the Earth-Moon barycenter and with the Sun located on the negative x-axis. It demonstrates the effect of the Sun's gravity on the perigee of an orbit about the secondary mass in the CRTBP. The solar perturbation of the two body elliptical orbit increases the perigee radius between the first and second flybys, labeled in Fig. 1 as perigee 1 and perigee 2, respectively. The magnitude of the third perigee is also greatly increased when compared to the first perigee. The periodic orbit has five perigees in total, with perigees 4 and 5 symmetric reflections of perigees 3 and 2, respectively. Table 1 compares the perigee radii of the three unique flybys. In Markellos's scaling of the Sun-Jupiter CRTBP, which differs from the scaling in Eq. 1, the orbit has the defining properties listed in Table 2.

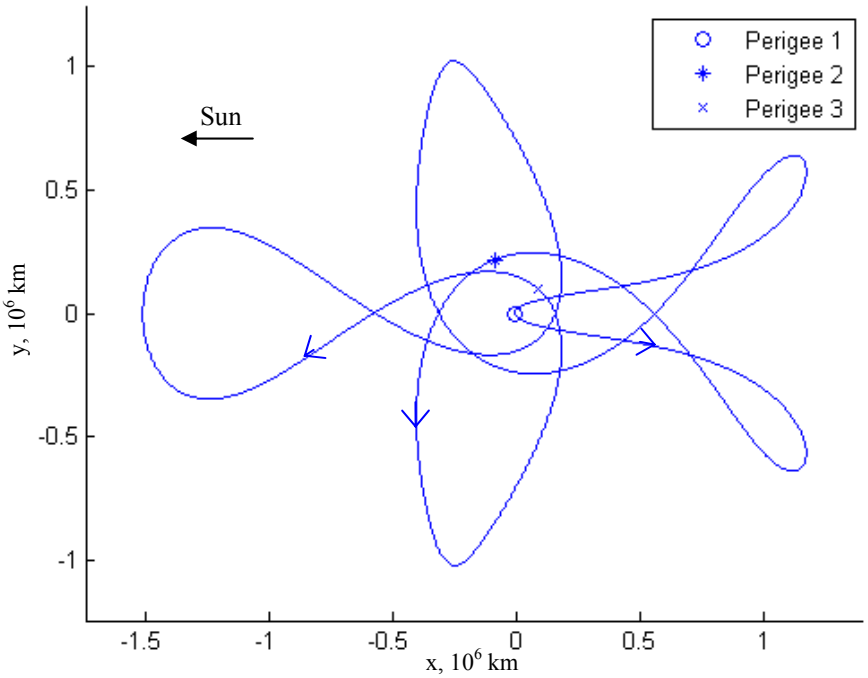

Fig. 1 Periodic orbit from Markellos's family *f*16 in rotating coordinates centered on the Earth-Moon combined mass

Table 1 Perigee distances in the orbit *f*16

perigee	radial distance (km)
1	7200
2	230434
3	132580

A similar periodic orbit can be found that is nearly a reflection of the orbit in Fig. 1 about the y-axis of the rotating coordinate system centered at the Earth-Moon combined mass. The orbit shown in Fig. 2, labeled here *f*'16, displays the same perigee raising characteristics as its counterpart in family *f*16.

An important characteristic of the orbits defined by families *f*16 and *f*'16 is that members of the family can be defined by a single parameter. For example, given a value for the nearest perigee radius that falls in the range of existence for the family, a unique member of the family can be defined. The orbits can therefore be scaled so that the nearest perigee may coincide with a pre-defined low Earth orbit. Similarly, the Jacobi constant of the orbit can be used as a defining parameter. Given a value of the Jacobi energy, a member of each family can be found.

Table 2 Properties of the *f*16 reference periodic orbit in Markellos's scaling units

initial x value	Jacobi constant
6.7356×10^{-2}	40.2055

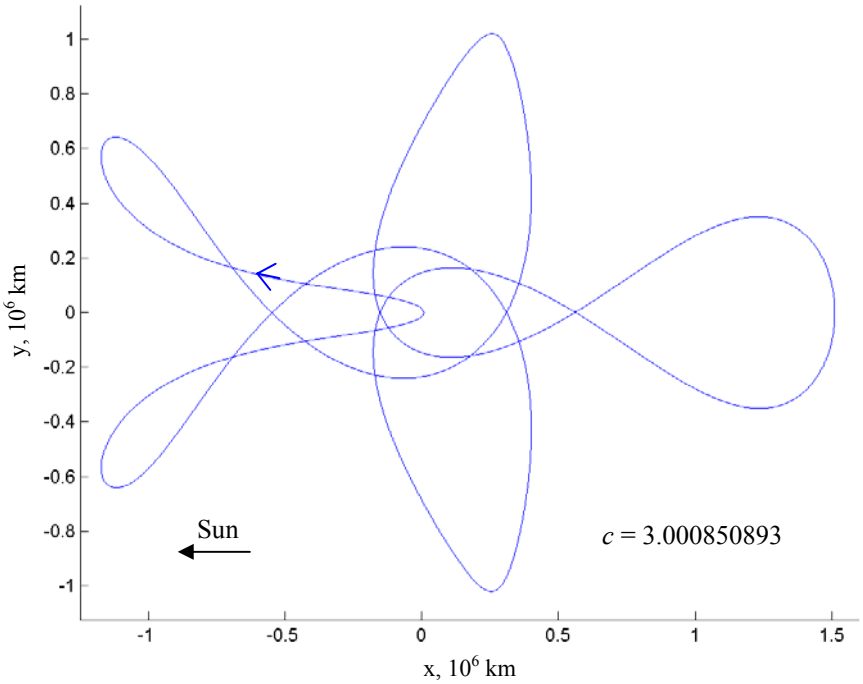

Fig. 2 Periodic orbit *f*'16 in rotating coordinates centered on the Earth-Moon combined mass

From Miele [18] and Szebehely, [16] an orbit in the CRTBP that makes two perpendicular crossings of the x-axis is necessarily periodic due to the symmetries of the system. Both of the orbits detailed cross the x-axis perpendicularly at their nearest and farthest points from the secondary body. These periodic orbits are 5-periodic orbits of the second kind, crossing the x-axis five times before the periodicity is established with a perpendicular intersection with the x-axis.

Periodic orbits of this type can be easily found using differential correction [19]. The trajectory begins at the nearest perigee, located on the x-axis with velocity perpendicular to the x-axis. The trajectory is propagated from that point with an initial velocity that yields an appropriate Jacobi constant until the x-axis is crossed five times. The initial velocity is then adjusted through an iterative process to yield a trajectory that has zero velocity in the x-direction at the 5th crossing of the x-axis. The converged initial conditions are then propagated forward for twice the amount of time, and the periodic orbit is established.

Reference Trajectory Selection for Ballistic Lunar Capture Targeting

As detailed in Table 1, this periodic orbit can be used to increase the perigee of a spacecraft's orbit without a maneuver. The reference trajectory for the ballistic lunar capture targeting algorithm will begin with an insertion into a family member of the shown periodic orbits at the nearest perigee, labeled perigee 1 in Fig. 1, and end at one

of the other perigees. The periodic orbit will be selected from family *f*16 or f'16 to coincide at the nearest perigee with the radius of the parking orbit of the satellite. Any of the perigees along the periodic orbit that have had their radii increased could then be used to target ballistic lunar capture trajectories. The work in this paper, however, covers only examples for achieving capture at the first and second perigees. If the first perigee is targeted, the transfer trajectory from low Earth orbit (LEO) to lunar orbit will have a period of approximately 100 days, and the reference trajectory is shown in bold in Fig. 3. The reference trajectory shown in Fig. 3 is labeled *f'16p1* to denote that it is from the generating family *f'*16 and targets a capture at the first increased perigee. In the case of targeting the second perigee, the period becomes approximately 180 days, and the reference trajectory, shown in Fig. 4, is labeled *f'16p2* due to its generating family and its target for capture at the second perigee. It should be noted that none of the perigee radii in the periodic orbits are equal to, or even closely approximate, the lunar distance from the Earth. These trajectories make suitable reference orbits because they display the dynamics necessary for the perigee to increase. Converged solutions that resulted from the reference trajectories of the two different periods are shown in Fig. 5 and Fig. 6. The solutions are not geometrically identical to the reference trajectories. The periodic orbits simply provide initial guesses that reliably allow convergence to ballistic lunar capture transfers. The selection of the appropriate periodic orbit for the reference trajectory from the generating families *f*16 and *f'*16 will be discussed in a following section.

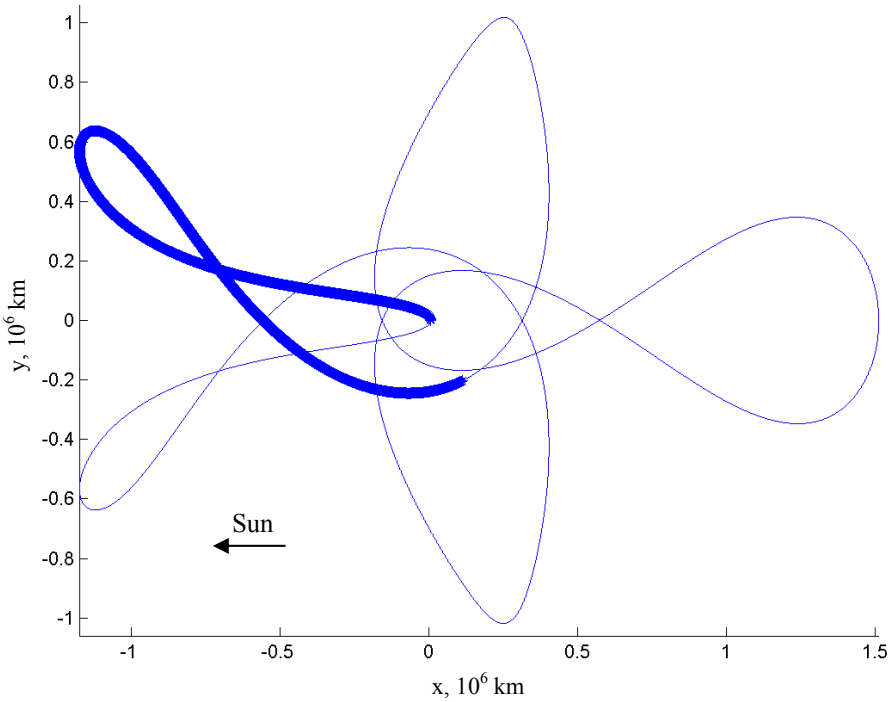

Fig. 3 Reference trajectory for a *f'16p1* transfer in rotating coordinates centered on the Earth-Moon combined mass

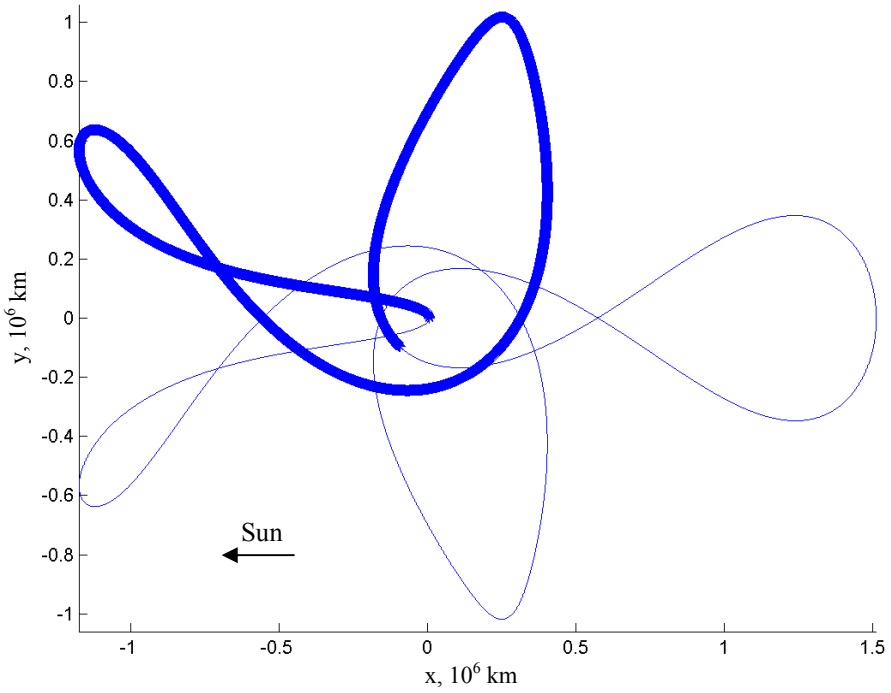

Fig. 4 Reference trajectory for a *f'16p2* transfer in rotating coordinates centered on the Earth-Moon combined mass

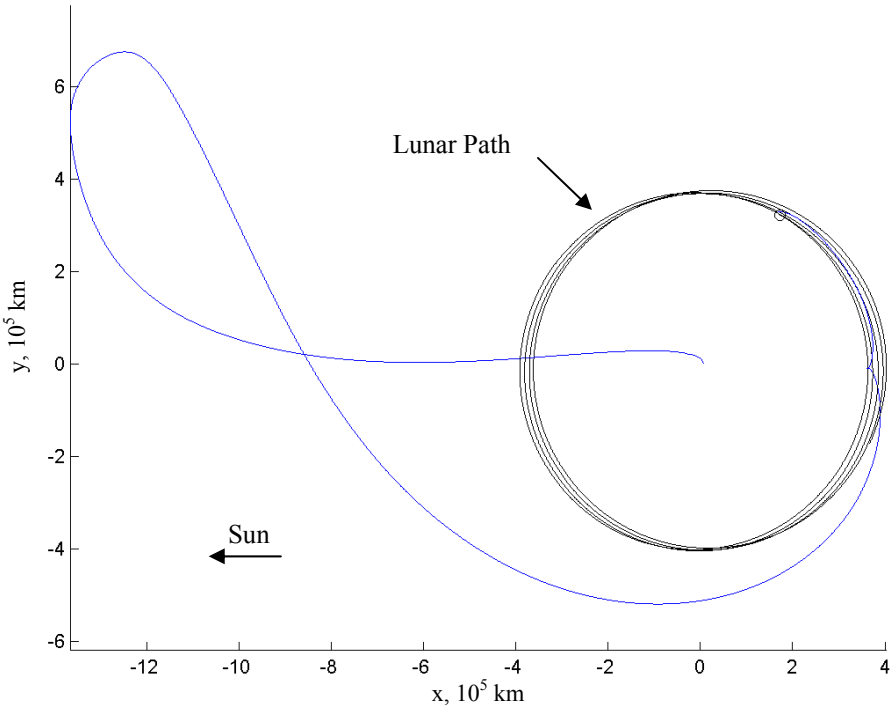

Fig. 5 A *f'16p1* transfer in Earth centered Sun-Earth rotating coordinates

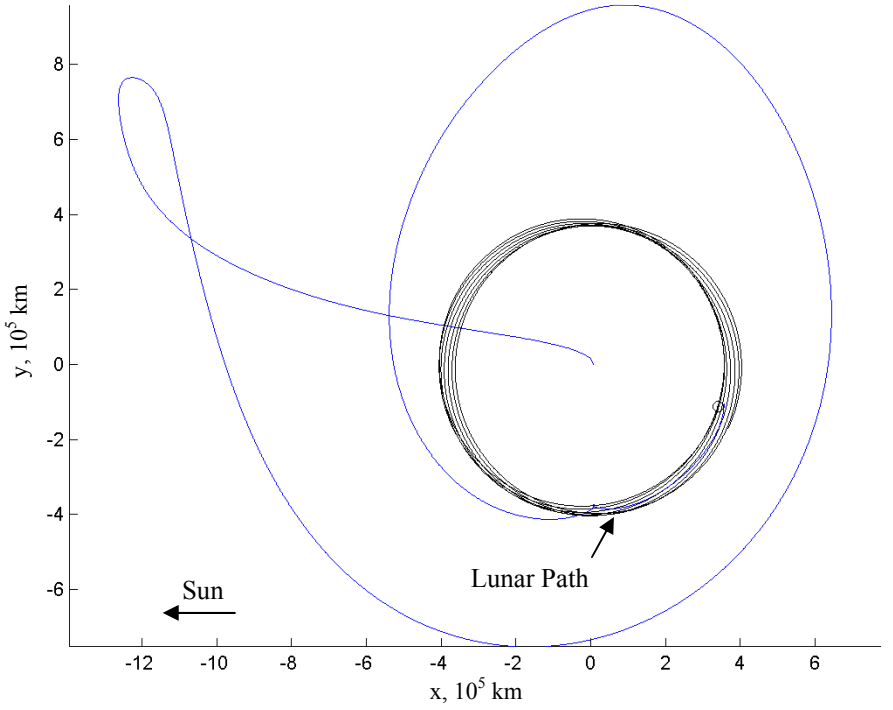

Fig. 6 A *f'16p2* transfer in Earth centered Sun-Earth rotating coordinates

Targeting Algorithm

An algorithm to incrementally step from the reference trajectory presented above to a ballistic lunar capture trajectory in a real world model is presented here. An incremental approach is used to increase the stability and reliability of the algorithm. In each step, elements of the real world system are added, increasing the complexity of the dynamics from the CRTBP used in the formulation of the reference trajectory. In this algorithm, the radius of the initial parking orbit and the desired initial time of the transfer are given parameters. The converged solution provides the orientation of the parking orbit and the ΔV that will result in a captured lunar orbit.

Transfer Orientation

The initial task of the targeting algorithm is to select the proper family of generating obits from the two generating families, *f*16 and *f*16'. One of the factors of the reliability of the targeting algorithm is the effect of the Moon's gravity on the outbound leg of the ballistic lunar capture trajectory. Depending on the orientation of the Moon with respect to the trajectory, the lunar perturbation can vary greatly. To increase the stability of the algorithm, a transfer orientation with the farthest distance from the Moon is chosen in order to mitigate the effect of the Moon on this leg of the transfer. Trajectories that employ a lunar flyby on the outbound segment can have advantages in cost savings, but are not presented here.

Insertion into either of the two possible transfers can be achieved with a ΔV in the direction of the velocity vector of the spacecraft in a prograde low Earth parking orbit. The selection of the appropriate class of trajectory to target on a given launch date is made based on the location of the Moon in the Sun-Earth rotating coordinate frame at the time of the transfer. If the Moon is located in the quadrants of the coordinate system farthest from the Sun, then the *f*'16 generating family should be used, maximizing the distance between the Moon and the spacecraft. If the Moon is located in a quadrant nearest to the Sun, then the generating family *f*16 is appropriate. Fig. 7 and Fig. 8 illustrate the selection of the reference trajectory. In the example ballistic lunar capture trajectory described below, the family *f*'16 is appropriate for the given epoch.

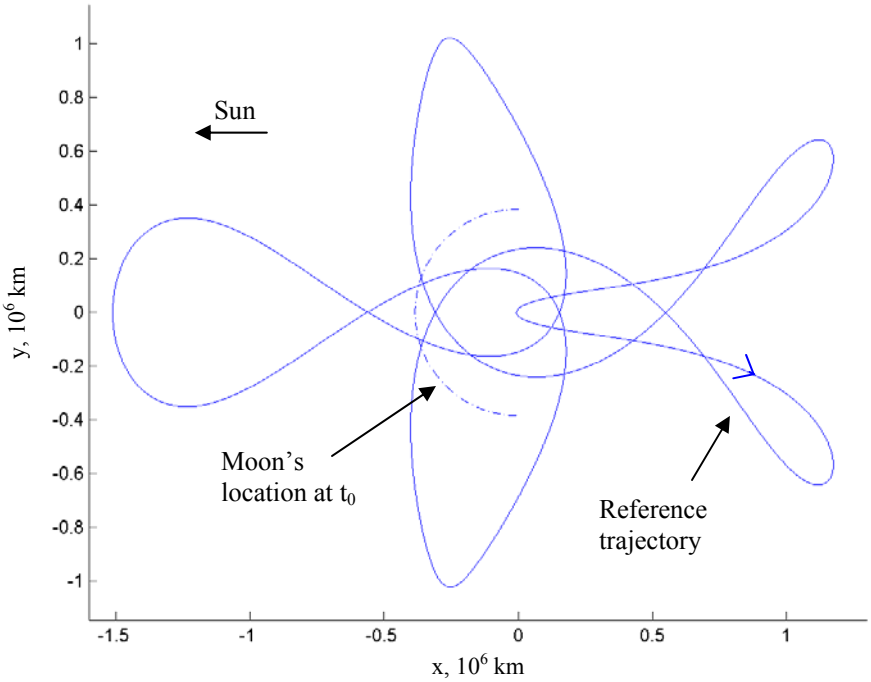

Fig. 7 Lunar position for generating family *f*16 selection in Earth centered rotating coordinates

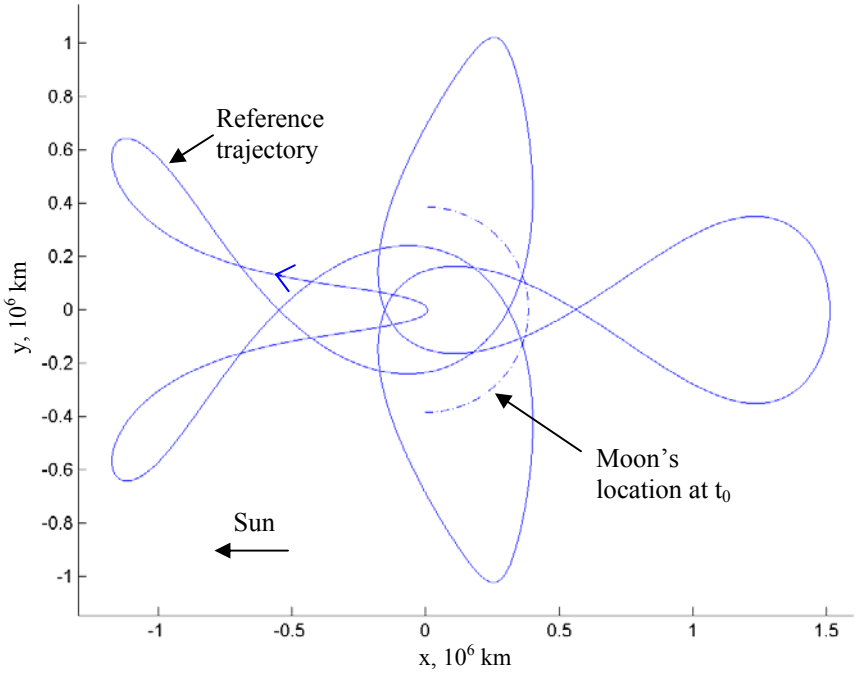

Fig. 8 Lunar position for generating family *f*'16 selection in Earth centered rotating coordinates

Estimation of Transfer Time

The next step in the targeting algorithm is to estimate the transfer time. The initial time is provided among the given parameters in the problem statement. The final time is set to coincide with one of the Moon's crossings of the

y-z plane in the Earth-Sun rotating coordinates centered on the Earth. Because the Moon's orbit is out of plane in the rotating coordinate system, there are two crossings of the y-z plane each month, one in the positive-y direction and one in the negative-y direction. The appropriate crossing is selected to coincide with the reference trajectory. For example, in the *f'16* trajectories the appropriate final time is the time of the Moon's passage from the third quadrant to the fourth quadrant of the rotating coordinate system shown in Fig. 8. In order to allow for the appropriate phasing, the final time is selected to be that of the crossing that occurs nearest to 100 days from the given initial time.

Regardless of the initial time, the final time will be chosen based on the orientation of the Moon in rotating coordinates. By following this procedure, the initial time is arbitrary, but a spacecraft will arrive at the Moon at one of two possible times during each month.

ΔV Targeting in the Restricted Three Body Problem

With an estimation of the transfer time, the first targeting step can be performed. Following the method developed by Pu and Edelbaum, [20] an approximate ΔV_0 for the four body problem is calculated in a three body problem by adding the mass of the Moon to the mass of the Earth. The combined mass is located at the Earth-Moon barycenter. The radius of the initial parking orbit is then adjusted to produce the same circular velocity around the combined mass object as the original parking orbit around the Earth as shown in Eq. 4.

$$r_2 = r_1 \frac{\mu_e + \mu_m}{\mu_e} \tag{4}$$

This three body problem allows a good approximation of the ΔV required to insert the spacecraft into the transfer. An initial guess of the ΔV is determined by taking the difference between the spacecraft's circular velocity and its velocity at the closest flyby on the reference trajectory. For this step, the orientation of the parking orbit is fixed in the orbital plane of the Earth-Moon barycenter around the Sun, and only the magnitude of the initial burn is varied. The ΔV is assumed to be oriented in the direction of the spacecraft's velocity vector.

In the numerical propagation of the trajectory, the Sun and the Earth-Moon combined masses are both treated as point masses. Their locations are determined from the JPL DE405 [21] ephemeris. The trajectory of the spacecraft is propagated in a non-rotating coordinate frame centered on the Earth-Moon combined mass, and the motion in the restricted three body problem (RTBP) is governed by Eq. 5.

$$\ddot{\mathbf{r}}_{RTBP} = -\frac{\mu_e + \mu_m}{r^3}\mathbf{r} - \frac{\mu_s}{r_{sc/s}^3}\mathbf{r}_{sc/s} - \frac{\mu_s + \mu_e + \mu_m}{r_s^3}\mathbf{r}_s \tag{5}$$

A differential correction algorithm is used in this targeting step. In the interest of relating this step to following steps, the algorithm is defined as follows. Let $\mathbf{x}_p$ be the vector of parameters that are varied to satisfy the targeting constraints. The vector **c** contains the constraints that must be driven to zero in the numerical routine. The differential correction algorithm estimates the derivative of $\mathbf{x}_p$ with respect to **c** in order to find the correction of $\mathbf{x}_p$ to make **c** approach the zero vector.

For this targeting step, there is only one free parameter, $x_p = \Delta V$. The target is the spacecraft's crossing of the y-z plane of the Earth-Moon barycenter centered, Sun-combined mass rotating coordinate system at t_f, $c = r_x$. The transversal of the y-z plane will occur in the bottom half of the x-y plane if observed from above, resulting in a trajectory similar to the trajectory shown in Fig. 9.

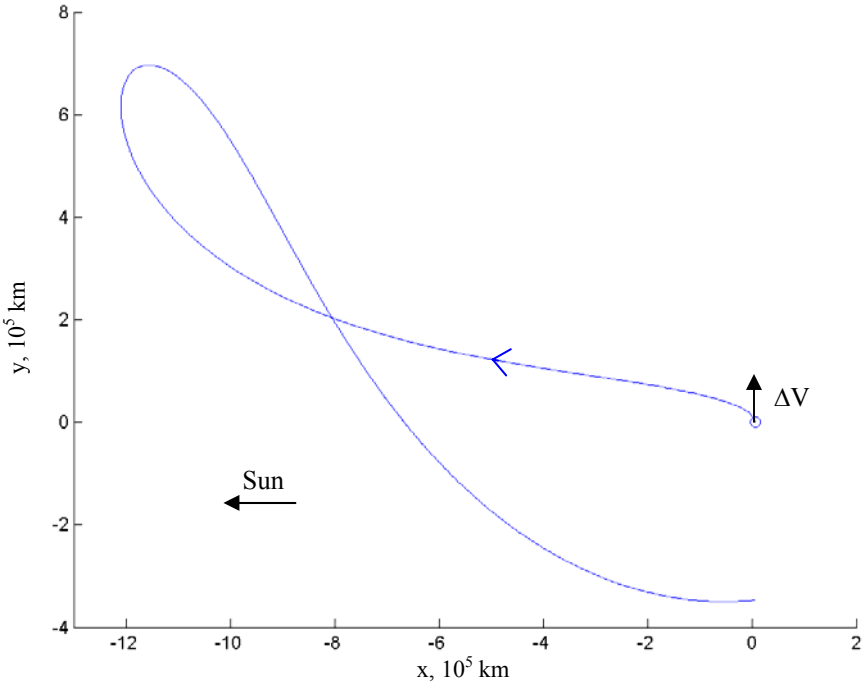

Fig. 9 Crossing of the y-axis in rotating coordinates centered on the Earth-Moon combined mass

As can be seen in Fig. 9, the solar influence on the orbit has raised the orbit's perigee at the second flyby. Table 3 details the parameters of the first iteration step for the sample trajectory shown in Fig. 9.

Table 3 First iteration step

	t_0 (Julian date)	parking orbit radius (km)	ΔV (km/s)	Δt (days)
initial	2453611	7200	3.08568	87.42570
solution	2453611	7200	3.04789	87.42570

Parking Orbit Orientation Selection in the Restricted Three Body Problem

With the result obtained above, the approximate ΔV has been established for the ballistic lunar capture trajectory. Continuing with Pu and Edelbaum's approximation of the four body problem, the approximate orientation of the initial parking orbit should be obtained before attempting to propagate the trajectory in the more complicated four body dynamical system.

Let α, β and γ be the orientation angles for the parking orbit. These angles define the position of a spacecraft in a circular orbit of given radius, and are analogous to the inclination, longitude of the ascending node, and true anomaly, respectively. They differ from orbital elements only in that they are defined relative to the x-y plane of the solar system as opposed to the equatorial plane of the Earth. In the targeting algorithm, the orientation angles represent the orientation of the spacecraft at the time of the transfer insertion burn. The transformation from a set of orientation angles to Cartesian coordinates is shown in Eq. 6.

$$\begin{aligned}\mathbf{r} &= r\begin{pmatrix}\cos\beta\cos\alpha-\sin\beta\sin\alpha\cos\gamma\\ \cos\beta\sin\alpha+\sin\beta\cos\alpha\cos\gamma\\ \sin\beta\sin\gamma\end{pmatrix}\\ \mathbf{v} &= \sqrt{\frac{\mu}{r}}\begin{pmatrix}-\cos\alpha\sin\beta-\cos\beta\sin\alpha\cos\gamma\\ -\sin\alpha\sin\beta+\cos\beta\cos\alpha\cos\gamma\\ \sin\gamma\cos\beta\end{pmatrix}\end{aligned} \tag{6}$$

Using the definition of the correction scheme described above, the four free variables in Eq. 7 are iterated from their values that were used in the last targeting step to target a point on the y-axis in the Sun-(Earth-Moon) rotating coordinate system. The target should be at a distance from the combined Earth-Moon mass equal to the distance from the Earth to the collinear Lagrange point of the Earth-Moon three body system exterior to the Moon, $\mathbf{c} = \mathbf{r} - \mathbf{r}_{L2}$. In this iteration step, four parameters are used to target a three dimensional point.

$$\mathbf{x}_p = \begin{pmatrix}\Delta V & \alpha & \beta & \gamma\end{pmatrix}^T \tag{7}$$

The result of the previous iterations should provide approximate solutions for the orientation of the spacecraft at the time of the transfer insertion burn as well as the magnitude of the burn, which is oriented along the direction of the velocity vector of the spacecraft. The approximation is satisfactorily accurate to converge to a solution in the complex dynamics of the Sun-Earth-Moon four body problem. Table 4 details the results of the second iteration step, continuing the targeting of the example trajectory in Fig. 9.

Table 4 Second iteration step results

	t_0 (Julian date)	α (rad)	β (rad)	γ (rad)	ΔV *(km/s)*	Δt *(days)*
initial	2453611	0.00000	2.70878	0.40907	3.04789	87.42570
solution	2453611	0.62247	1.78275	0.35308	3.04889	87.42570

Targeting in the Restricted Four Body Problem

At this stage of the algorithm, the masses of the Moon and the Earth are decoupled, and a more realistic system is used. The numerical stability of any targeting algorithm continues to be an issue, and the ballistic lunar capture trajectory is targeted in two steps.

The four free parameters used in the previous targeting step are used again in the four body system. Equations of motion governing the four body problem are now used. The three gravitational bodies are treated as point masses located at positions determined from the JPL DE405 ephemeris. The coordinate system in which the trajectory is propagated is a non-rotating frame centered at the Earth-Moon barycenter. Eq. 8 shows the restricted four body problem equations of motion with an indirect term to account for the acceleration of the origin of the coordinate system.

$$\ddot{\mathbf{r}}_{RFBP} = -\frac{\mu_e}{r_{sc/e}^{\ 3}}\mathbf{r}_{sc/e} - \frac{\mu_m}{r_{sc/m}^{\ 3}}\mathbf{r}_{sc/m} - \frac{\mu_s}{r_{sc/s}^{\ 3}}\mathbf{r}_{sc/s} - \frac{\mu_s + \mu_e + \mu_m}{r_s^{\ 3}}\mathbf{r}_s \tag{8}$$

The target in this iteration is the spacecraft's radial distance from the Moon. The iteration is considered successful if the final radial distance from the Moon is less than the distance from the Moon to L2 of the Earth-Moon three body system. In this case the constraint is an inequality constraint, $r_{sc/m} \le r_{L_2/m}$. The parameter vector $\mathbf{x}_p$ is the same as the previous targeting step, Eq. 7. Table 5 shows the details of the four body targeting step.

Table 5 Restricted four body targeting step

	t_0 (Julian date)	α (rad)	β (rad)	γ (rad)	ΔV *(km/s)*	Δt *(days)*
initial	2453611	0.62247	1.78275	0.35308	3.04889	87.42570
solution	2453611	1.31989	1.22746	0.40292	3.04932	87.42570

Energy Minimization in the Restricted Four Body Problem

The final step of the targeting algorithm is a constrained minimization of the spacecraft's Keplerian energy with respect to the Moon. In this minimization step, let $J = KE_m$ be the scalar performance index to be minimized by a sequential quadratic programming algorithm [22]. The final time of the transfer is included with the initial time and the orientation angles of the parking orbit as free variables, shown in Eq. 9.

$$\mathbf{x}_p = \begin{pmatrix} \Delta V & \alpha & \beta & \gamma & t_f \end{pmatrix}^T \tag{9}$$

The constraint in this step forces the trajectory to end at a perilune. This constraint, $c = f_m$, aids in convergence to trajectories that do not crash into the Moon and complete an orbit of the Moon without escaping. If desired, an additional inequality constraint may be added to ensure the perilune distance is sufficient to avoid collision with the lunar surface.

After a few iterations, the minimization results in a negative Keplerian energy, and thus a captured orbit around the Moon. If a particular orbit around the Moon is desired, constraints can be added to the minimization problem that will yield the desired orbit, possibly with another small burn. The results of the targeting algorithm are shown in Table 6, and the capture trajectory is displayed in Fig. 5. It is noteworthy that the trajectory already possesses negative energy with respect to the Moon before this iteration step; however, the minimization of energy is necessary to produce a trajectory that remains captured by the Moon for a significant period of time.

Table 6 Minimization of Keplerian energy

	t_0 (Julian date)	α (rad)	β (rad)	γ (rad)	ΔV (km/s)	Δt (days)	KE (km^2/s^2)
initial	2453611	1.31989	1.22746	0.40292	3.04932	87.42570	-0.05379
solution	2453611	1.36268	1.14152	0.40272	3.04971	99.03939	-0.10498

Success Criteria

A successful targeting algorithm will systematically produce captured trajectories. In a multibody system, however, the definition of capture is problematic. In the two body problem, a negative Keplerian energy is sufficient for ensuring the spacecraft will not escape the system. Similarly, in the restricted three body problem a Jacobi energy value that produces zero velocity surfaces that constrain the motion of the spacecraft to one of the primary bodies is an identifier of a captured spacecraft. In the four body problem used in the targeting algorithm, there are no constant energy-like quantities that bind the motion of the spacecraft. This problem has been previously dealt with in

several ways. Belbruno, in defining the weak stability boundary, defines a weakly captured trajectory as a trajectory that completes an orbit of a body, returning to the vertical plane from which it began, with negative Keplerian energy [1]. In finding WSB transfers using manifolds in the restricted three body problem, Koon et al. define a successful transfer as one that transits through the halo orbit into the system of the secondary body [5].

The following three metrics for evaluating the capture of a spacecraft into lunar orbit are proposed to evaluate the success of the targeting algorithm. At the conclusion of the final step of the algorithm the trajectory is at a perilune. Although termination at perilune is not required in the algorithm to have negative Keplerian energy with respect to the Moon, a successfully captured trajectory should have negative energy at this point. The first metric used to evaluate the algorithm is whether a solution is found that has negative Keplerian energy with respect to the Moon at this point. Furthermore, a second, more stringent metric is used that demands a binding of the motion of the spacecraft to the Moon. Under the second metric, the algorithm is considered to be successful if there is a second perilune with negative Keplerian energy as the trajectory is propagated forward, ensuring an orbit of the Moon. Finally, a third metric is used to ensure against collision. Under this metric, the algorithm is deemed to be successful if it meets the previous two requirements, and the perilune radii are greater than the Moon's radius.

State Transition Matrix Based Derivatives

The algorithm described above relies on a differential correction algorithm and a sequential quadratic programming routine. These methods require the calculation of the derivatives of the target parameters with respect to the free variables. Traditionally, finite difference methods have been used in the correction and minimization procedures. An alternative approach using analytical gradients computed via the state transition matrix is presented here in an attempt to maximize the accuracy of the derivatives and therefore increase the likelihood of convergence.

Due to the chaotic nature of ballistic lunar capture trajectories, small changes in the initial state can lead to very large changes in the final state, making finite difference methods unreliable. The forward difference method has been shown to rely on the differencing of several integrations. Errors are introduced through integration error and the selection of the numerical step size. If it is too large, truncation errors dominate, while a step size that is too small results in round off errors. The appropriate selection of the step size can result in a partial derivative that is accurate to one half of the number of digits that the function is known [23].

Zimmer and Ocampo [24] have demonstrated the benefits in accuracy from using state transition matrix derivatives, as opposed to finite difference methods. First order derivatives relating the states at the initial time to the states at the final time can be calculated explicitly by solving for the state transition matrix. The state transition matrix relating to the propagation of a spacecraft through a central body force field can be solved for explicitly, and its derivatives are exact to first order. The dynamical models used in this algorithm do not yield explicit solutions to the state transition matrix, and therefore it must be numerically integrated. Error is introduced in the integration, but it is on the order of the error in the integration itself. The result is a more accurate representation of the required derivatives.

The state transition matrix of the three and four body problem is found by numerically integrating the relationship in Eq. 11, where F is the time dependent state propagation matrix for the desired dynamical model, shown in Eq. 12, where the state vector $\mathbf{X}$ is defined in Eq. 13.

$$\begin{aligned} \dot{\Phi}(t,t_0) &= F(t)\Phi(t,t_0) \\ \Phi(t_0,t_0) &= I \end{aligned} \tag{11}$$

$$F(t) = \frac{\partial \dot{\mathbf{X}}(t)}{\partial \mathbf{X}(t)} \tag{12}$$

$$\mathbf{X} = \begin{pmatrix} \mathbf{r} \\ \mathbf{v} \end{pmatrix} \tag{13}$$

The state propagation matrix for the three-body and four-body dynamical systems of interest to the algorithm are given in Eq. 14, where $\ddot{\mathbf{r}}$ is given in Eq. 5 for the three-body dynamical system and in Eq. 8 for the four-body dynamical system.

$$F(t) = \begin{pmatrix} 0 & I \\ \dfrac{\partial \ddot{\mathbf{r}}}{\partial \mathbf{r}} & 0 \end{pmatrix} \tag{14}$$

For the non-rotating restricted four body problem, the sub-matrix in Eq. 14 that represents the partial derivative of the acceleration vector with respect to the radius vector is written as

$$\left(\frac{\partial \ddot{\mathbf{r}}}{\partial \mathbf{r}}\right)_{RFBP} = \left(\frac{3\mu_e}{r^5}\right)\mathbf{r}\mathbf{r}^{\mathrm{T}} + \left(\frac{3\mu_m}{r_m{}^5}\right)\mathbf{r}_m\mathbf{r}_m{}^{\mathrm{T}} + \left(\frac{3\mu_s}{r_s{}^5}\right)\mathbf{r}_s\mathbf{r}_s{}^{\mathrm{T}} - \mathbf{I}\left(\frac{\mu_e}{r^3} + \frac{\mu_m}{r_m{}^3} + \frac{\mu_s}{r_3{}^3}\right), \tag{15}$$

while in the non-rotating restricted three body problem it is

$$\left(\frac{\partial \ddot{\mathbf{r}}}{\partial \mathbf{r}}\right)_{RTBP} = \left(\frac{3\mu_e}{r^5}\right)\mathbf{r}\mathbf{r}^{\mathrm{T}} + \left(\frac{3\mu_s}{r_s^5}\right)\mathbf{r}_s\mathbf{r}_s^{\mathrm{T}} - \mathbf{I}\left(\frac{\mu_e}{r^3} + \frac{\mu_s}{r_3^3}\right). \tag{16}$$

Perturbations in the free variables are related to perturbations in the constraint values using the chain rule. The targeting algorithm relies on partial derivatives relating both the final state and the final value of the Keplerian energy to the five control parameters listed in Eq. 9. For the orientation angle α, the partial derivatives are written in the form

$$\frac{\partial KE_f}{\partial \alpha} = \frac{\partial KE_f}{\partial \mathbf{X}_f}\frac{\partial \mathbf{X}_f}{\partial \mathbf{X}_0}\frac{\partial \mathbf{X}_i}{\partial \alpha} \tag{17}$$

and

$$\frac{\partial \mathbf{X}_f}{\partial \alpha} = \frac{\partial \mathbf{X}_f}{\partial \mathbf{X}_0}\frac{\partial \mathbf{X}_i}{\partial \alpha}, \tag{18}$$

where

$$\frac{\partial \mathbf{X}_f}{\partial \mathbf{X}_0} = \Phi\left(t_f, t_0\right), \tag{19}$$

$$\frac{\partial KE_f}{\partial \mathbf{X}_f} = \left(\frac{\mu_m}{r_m^3}\left(x - x_m\right) \quad \frac{\mu_m}{r_m^3}\left(y - y_m\right) \quad \frac{\mu_m}{r_m^3}\left(z - z_m\right) \quad v_x - v_{mx} \quad v_y - v_{my} \quad v_z - v_{mz}\right), \tag{20}$$

and

$$\frac{\partial \mathbf{X}_i}{\partial \alpha} = \begin{pmatrix} r\left(-\sin\alpha\cos\beta - \cos\alpha\sin\beta\cos\gamma\right) \\ r\left(\cos\alpha\cos\beta - \sin\alpha\sin\beta\cos\gamma\right) \\ 0 \\ v\left(\sin\alpha\sin\beta - \cos\alpha\cos\beta\cos\gamma\right) \\ v\left(-\cos\alpha\sin\beta - \sin\alpha\cos\beta\cos\gamma\right) \\ 0 \end{pmatrix}. \tag{21}$$

Similarly, the partial derivatives relating to the orientation angle β are written as

$$\frac{\partial KE_f}{\partial \beta} = \frac{\partial KE_f}{\partial \mathbf{X}_f}\frac{\partial \mathbf{X}_f}{\partial \mathbf{X}_0}\frac{\partial \mathbf{X}_i}{\partial \beta} \tag{22}$$

and

$$\frac{\partial \mathbf{X}_f}{\partial \beta} = \frac{\partial \mathbf{X}_f}{\partial \mathbf{X}_0}\frac{\partial \mathbf{X}_i}{\partial \beta} \tag{23}$$

where the partial derivative of the Keplerian energy with respect to the final state is given in Eq. 22, the partial derivative of the final state with respect to the initial state is given as the state transition matrix, and

$$\frac{\partial \mathbf{X}_i}{\partial \beta} = \begin{pmatrix} r\left(-\cos\alpha\sin\beta - \sin\alpha\cos\beta\cos\gamma\right) \\ r\left(-\sin\alpha\sin\beta + \cos\alpha\cos\beta\cos\gamma\right) \\ r\cos\beta\sin\gamma \\ -v\left(\cos\alpha\cos\beta - \sin\alpha\sin\beta\cos\gamma\right) \\ -v\left(\sin\alpha\cos\beta + \cos\alpha\sin\beta\cos\gamma\right) \\ -v\sin\alpha\sin\gamma \end{pmatrix}. \tag{24}$$

The partial derivatives relating to the orientation angle γ are

$$\frac{\partial KE_f}{\partial \gamma} = \frac{\partial KE_f}{\partial \mathbf{X}_f}\frac{\partial \mathbf{X}_f}{\partial \mathbf{X}_0}\frac{\partial \mathbf{X}_i}{\partial \gamma} \tag{25}$$

and

$$\frac{\partial \mathbf{X}_f}{\partial \gamma} = \frac{\partial \mathbf{X}_f}{\partial \mathbf{X}_0}\frac{\partial \mathbf{X}_i}{\partial \gamma} \tag{26}$$

where the partial derivative of the Keplerian energy with respect to the final state is given in Eq. 22, the partial derivative of the final state with respect to the initial state is given as the state transition matrix, and

$$\frac{\partial \mathbf{X}_i}{\partial \gamma} = \begin{pmatrix} r\sin\alpha\sin\beta\sin\gamma \\ -r\cos\alpha\sin\beta\sin\gamma \\ r\sin\beta\cos\gamma \\ v\left(\sin\alpha\cos\beta\sin\gamma\right) \\ -v\left(\cos\alpha\cos\beta\sin\gamma\right) \\ v\cos\beta\cos\gamma \end{pmatrix}. \tag{27}$$

The initial maneuver produces the partial derivatives

$$\frac{\partial KE_f}{\partial \Delta V} = \frac{\partial KE_f}{\partial \mathbf{X}_f}\frac{\partial \mathbf{X}_f}{\partial \mathbf{X}_0}\frac{\partial \mathbf{X}_i}{\partial \Delta V} \tag{28}$$

and

$$\frac{\partial \mathbf{X}_f}{\partial \Delta V} = \frac{\partial \mathbf{X}_f}{\partial \mathbf{X}_0}\frac{\partial \mathbf{X}_i}{\partial \Delta V} \tag{29}$$

where the partial derivative of the Keplerian energy with respect to the final state is given in Eq. 22, the partial derivative of the final state with respect to the initial state is given as the state transition matrix, and

$$\frac{\partial \mathbf{X}_i}{\partial \Delta V} = \begin{pmatrix} \mathbf{0}_{3x1} \\ \Delta V\left(-\cos\alpha\sin\beta - \sin\alpha\cos\beta\cos\gamma\right) \\ \Delta V\left(-\sin\alpha\sin\beta + \cos\alpha\cos\beta\cos\gamma\right) \\ \Delta V\cos\beta\sin\gamma \end{pmatrix}. \tag{30}$$

Finally, the partial derivative of the final state with respect to the final time does not include the state transition matrix.

$$\frac{\partial KE_f}{\partial t_f} = \frac{\partial KE_f}{\partial \mathbf{X}_f}\frac{\partial \mathbf{X}_f}{\partial t_f} \tag{31}$$

where

$$\frac{\partial \mathbf{X}_f}{\partial t_f} = \begin{pmatrix} \mathbf{v}_f \\ \mathbf{a}_f \end{pmatrix} \tag{32}$$

and $\mathbf{a}_f$ is defined in Eq. 8 for the four body problem and Eq. 5 for the three body problem.

Results

Low energy transfers are shown to be found in a systematic way when periodic orbits in the CRTBP are used to initialize the algorithm. To validate the robustness of the technique, a computer program was designed to implement the algorithm described above with the goal of computing a low energy lunar transfer on a user supplied date. Transfers of class *f16p1* and *f'16p1* were computed in an automated way. The program was then supplied with a randomly generated date and time between January 1, 2010 and January 1, 2012, and a low energy lunar transfer was calculated for that date. The program was fed 1000 randomly generated dates and times. The results of the run are shown in Table 7.

Table 7 Algorithm results

Number of Runs	Criteria 1 (negative energy)	Criteria 2 (orbit)	Criteria 3 (orbit, no collision)
1000	100%	96.50%	91.10%

Software Models

The numerical trajectory propagation was performed assuming the gravitational bodies act as point masses. Unless otherwise noted, the locations of the point masses were determined using the DE405 ephemeris. The equations of motion as described in the preceding sections are integrated using DLSODA [25]. For both the numerical nonlinear equation solving and minimization functions, VF13AD was used. In all simulations, the values of the gravitational parameters used are listed in Table 8.

Table 8 Gravitational parameter values

Gravitational Parameter	Value (km^3/sec^2)
μ_s	1.32715×10^{11}
μ_e	3.986004×10^{5}
μ_m	4.9029×10^{3}

Conclusions

An efficient, robust method of targeting ballistic lunar capture trajectories is presented. The use of a periodic trajectory from family *f*16 in the circular restricted three body problem with the Sun as the primary mass and an Earth-Moon combined body as the secondary mass demonstrates the solar effect in raising the perigee of the spacecraft's orbit to approximately lunar radius. This reference trajectory serves as an excellent initial guess in the targeting algorithm that produces ballistic lunar capture trajectories on arbitrary launch dates and times. The numerical difficulties of targeting chaotic trajectories in the Sun-Earth-Moon four body problems are effectively handled by the use of precise gradients obtained through the numerical propagation of the state transition matrix.

References

[1] Belbruno, E. A., "Lunar Capture Orbits, A Method of Constructing Earth-Moon Trajectories and the Lunar GAS Mission," AIAA Paper 87-1054, May 1987.

[2] Belbruno, E. A., and Miller, J. K., "Sun-Perturbed Earth-to-Moon Transfers with Ballistic Capture," *Journal of Guidance, Control, and Dynamics*, Vol. 16, No. 4, pp. 770-775.

[3] Belbruno, E. A., and Carrico, J. P., "Calculation of Weak Stability Boundary Ballistic Lunar Transfer Trajectories," AIAA Paper 2002-4142, August 2000.

[4] Yamakawa, H., Kawaguchi, J., Ishii, N., and Matsuo, H., "A Numerical Study of Gravitational Capture Orbit in the Earth-Moon System," AAS Paper 92-186, Feb. 1992.

[5] Koon, W. S., Lo, M. W., Marsden, J. E., and Ross, S. D., "Low Energy Transfer to the Moon," *Celestial Mechanics and Dynamical Astronomy*, Vol. 81, No. 1-2, September 2001, pp. 63-73.

[6] Yamato H., and Spencer, D. B., "Transit-Orbit Search for Planar Restricted Three-Body Problems with Perturbations," *Journal of Guidance, Control, and Dynamics*, Vol. 27, No. 6, Nov.-Dec. 2004, pp. 1035-1045.

[7] Parker, J. S., and Lo, M. W., "Families of Low-Energy Lunar Halo Orbit Transfers," AAS Paper 06-132, February 2006.

[8] Biesbroek, R. G. J., Ockels, W. J., and Janin, G., "Optimisation of Weak Stability Boundary Orbits from GTO to the Moon Using Genetic Algorithms," IAF Paper No. 99-A.6.10, Oct. 1999.

[9] Yagasaki, K., "Sun-Perturbed Earth-to-Moon Transfers with Low Energy and Moderate Flight Time," *Celestial Mechanics and Dynamical Astronomy*, Vol. 90, No. 3-4, 2004, pp. 197-212.

[10] Bollt, E. M., and Meiss, J. D., "Targeting Chaotic Orbits to the Moon Through Recurrance," *Physics Letters A*, Vol. 204, No. 5-6, 1995, pp. 373-378.

[11] Macau, E. E. N., and Grebogi, C., "Control of chaos and its relevancy to spacecraft steering," *Philosophical Transactions of the Royal Society A*, Vol. 364, No. 1846, 2006, pp. 2463-2481.

[12] Mengali, G., and Quarta, A. A., "Optimization of Biimpulsive Trajectories in the Earth–Moon Restricted Three-Body System," *Journal of Guidance, Control, and Dynamics*, Vol. 28, No. 2, 2005, pp 209-216.

[13] Ivashkin, V. V., "On the Moon-to-Earth Trajectories with Gravitational Escape from the Moon Attraction," *Doklady Physics*, Vol. 49, Issue 9, Sept. 2004, pp. 539-542.

[14] Lidov, M. L., "The evolution of orbits of artificial satellites of planets under the action of gravitational perturbations of external bodies," *Planetary and Space Science*, Vol. 9, Issue 10, pp. 719-759.

[15] Markellos, V. V., "Numerical Investigation of the Planar Restricted Three Body Problem," *Celestial Mechanics and Dynamical Astronomy*, Vol. 10, No. 1, August 1974, pp 87-134.

[16] Szebehely, V., *Theory of Orbits*, Academic Press, New York, 1967.

[17] Poincaré, H., *Les Méthodes Nouvelles de la Mécanique Céleste*, Vol. 1,2,3. Gauthier-Villars, Paris, 1892; reprinted by Dover, New York, 1957.

[18] Miele, A., "Theorem of Image Trajectories in the Earth-Moon Space," *Astronautica Acta*, Vol. 6, No. 225, 1960, pp. 225-232.

[19] Battin, R. H., *An Introduction to the Mathematics and Methods of Astrodynamics*, American Institute of Aeronautics and Astronautics, Inc., Virginia, 1999.

[20] Pu, C. L., and Edelbaum, T. N. "Four-Body Trajectory Optimization," *AIAA Journal*, Vol. 13, No. 3, Mar. 1975, pp. 333-336.

[21] Standish, E. M., "JPL Planetary and Lunar Ephemerides, DE405/LE405," Jet Propulsion Laboratory Interoffice Memorandum 312.F-98-048, August 26, 1998.

[22] "VF13AD", Harwell Subroutine Library ,URL: http://hsl.rl.ac.uk/archive/hslarchive.html

[23] Gill, P., Murray, W., and Wright, M. H., *Practical Optimization*, Academic Press, London, 1981, Chap. 8.

[24] Zimmer, S., and Ocampo, C., "Analytical Gradients for Gravity Assist Trajectories Using Constant Specific Impulse Engines," *Journal of Guidance, Control, and Dynamics*, Vol. 28, No. 4, Jul.–Aug. 2005, pp. 753-760.

[25] Hindmarsh, A. C., "Large Ordinary Differential Equation Systems and Software," *IEEE Control Systems Magazine*, Vol. 2, No. 4, 1982, pp. 24-30.